A large-area strain sensing technology for monitoring fatigue cracks in steel bridges

Xiangxiong Kong [a], Jian Li [a]*, William Collins [a], Caroline Bennett [a], Simon Laflamme [b,c], and Hongki Jo[d]

a Department of Civil, Environmental and Architectural Engineering,
University of Kansas, Lawrence, KS 66045, USA
b Department of Civil, Construction, and Environmental Engineering,
Iowa State University, Ames, IA, 50011, USA
c Department of Electrical and Computer Engineering,
Iowa State University, Ames, IA, 50011, USA
d Department of Civil Engineering and Engineering Mechanics
University of Arizona, Tucson, AZ, 85721, USA

Abstract

This paper presents a novel large-area strain sensing technology for monitoring fatigue cracks in steel bridges. The technology is based on a soft elastomeric capacitor (SEC), which serves as a flexible and large-area strain gauge. Previous experiments have verified the SEC's capability to monitor low-cycle fatigue cracks experiencing large plastic deformation and large crack opening. Here an investigation into further extending the SEC's capability for long-term monitoring of fatigue cracks in steel bridges subject to traffic loading, which experience smaller crack openings. It is proposed that the peak-to-peak amplitude (pk-pk amplitude) of the sensor's capacitance measurement as the indicator of crack growth to achieve robustness against capacitance drift during long-term monitoring. Then a robust crack monitoring algorithm is developed to reliably identify the level of pk-pk amplitudes through frequency analysis, from which a Crack Growth Index (*CGI*) is obtained for monitoring fatigue crack growth under various loading conditions. To generate representative fatigue cracks in laboratory, loading protocols were designed based on constant ranges of stress intensity to limit plastic deformations at the crack tip. A series of small-scale fatigue tests were performed under the designed loading protocols with various stress intensity ratios. Test results under the realistic fatigue crack conditions demonstrated the proposed crack monitoring algorithm can generate robust *CGIs* which are positively correlated with crack lengths and independent from loading conditions.

Keywords: fatigue crack; sensing skin; structural health monitoring; capacitive strain sensor; soft elastomeric capacitor; high-cycle fatigue; steel bridges; power spectral density, crack detection

*Assistant Professor; Email: jianli@ku.edu

1. Introduction

Fatigue cracks that develop in steel highway bridges under repetitive, traffic loading are one of the major mechanisms that degrades structural integrity. If bridges are not appropriately inspected and maintained, fatigue cracks can eventually lead to catastrophic failures, in particular for fracture-critical bridges [1]. It is critical to detect fatigue cracks at an early stage so that appropriate maintenance actions can be taken. Currently, visual inspection is the most frequently adopted approach for detecting cracks in highway bridges in the United Sates [2]. However, this method is costly, labor intensive, and prone to errors due to variations of inspector's skill for result interpretation [3]. Many advanced crack detection technologies have been proposed for monitoring fatigue crack initiation and/or propagation, including: acoustic emission [4], piezoelectric sensor [5], lamb wave [6], vibration analysis [7], and computer vision-based methods [8, 9, 10]. Nevertheless, complex setups, data processing algorithms, and noise sensitivity are among the challenges associated with use of these methods. A comprehensive literature review of advanced crack detection methods can be found in [11].

Direct strain measurement can be used for monitoring fatigue crack activity, and has the potential to offer effective detection of fatigue cracks if appropriately applied. If a crack occurs underneath or close to the sensor, the abrupt change in strain at the localized area can be detected. For this reason, both traditional foil-type strain gages [12] and fiber optic sensors [13] have been applied for crack detection. However, these sensors are generally small and have limited measurement ranges, and thus a large number of traditional strain sensors would be needed to monitor large structural surfaces, dramatically increasing cost and reducing practicality. In addition, these sensors are easily damaged under cracking due to their limited ductility, and thus cannot provide continuous monitoring after damage. Therefore, although conceptually straightforward, significant challenges still remain with using strain sensing elements to monitor fatigue cracks over large structural surfaces in a continuous manner.

In order to overcome these challenges researchers have attempted to deploy networks of large, flexible sensors. Such technology, analogous to a sensing skin, has been proposed to measure strain over large structural surfaces. Examples include carbon nanotube based sensors [14,15], resistive sensing sheets [16], printable conductive polymer [17], patch antenna sensors [18,19], and soft elastomeric capacitors (SECs) [20,21]. In particular, the SEC technology, previously developed by the authors, is highly scalable due to its ease of fabrication and use of low cost materials; additionally, SEC can be fabricated in large sizes. SECs are capable of unusually large deformations and a wide range of elastic strain measurement (up to 20% strain [22]). They are mechanically robust, making them suitable for long-term monitoring. Prior studies have demonstrated that SECs are able to monitor static [23] and dynamic [24] strain in various civil structural components and can monitor strain maps under in-plane stress conditions [25].

By overcoming the limitations associated with traditional strain sensors, SECs show great promise as part of a long-term robust fatigue crack monitoring system. Preliminary investigations [26,27,28] have demonstrated the SEC capability to detect and localize low-cycle fatigue cracks on compact

tension, *C(T)*, specimens. Moreover, a numerical approach based on finite element analysis [29,30] was established by the authors, enabling numerical prediction of the SEC's capacitance response in the presence of crack growth.

The objective of this study was to determine whether SECs are capable of being used as a fatigue monitoring device in common steel bridge applications. To accomplish this, the crack detection ability of the SEC was investigated in the context of high-cycle fatigue cracking, representative of cracking commonly encountered in steel bridges. Compared to low-cycle fatigue cracks, high-cycle fatigue cracks are generally subject to lower stress levels, are dominated by elastic deformation, and thus require a larger number of cycles to initiate and propagate. Importantly, crack openings under high-cycle fatigue are much smaller than those generated by low-cycle fatigue. As a result, monitoring high-cycle fatigue cracking with the SEC can be expected to be a more challenging proposition than monitoring low-cycle fatigue cracking, since the sensor should produce smaller responses under smaller crack openings. Long-term robustness is also critical to deploying an effective crack monitoring strategy in order to ensure functionality over the life of the structure being monitored.

To address these challenges, it was hypothesized that peak-to-peak amplitude (pk-pk amplitude) could be used as an indicator for monitoring crack growth, which would exhibit low sensitivity to capacitance drift. A crack monitoring algorithm based on frequency analysis was developed for accurately identifying the pk-pk amplitude and then calculating the Crack Growth Index (*CGI*). The approach relies on measurements from the SEC's response as well as the applied fatigue loading. Load can either be directly measured when possible in a laboratory setting or indirectly measured via structural strain in the field. To experimentally evaluate the proposed algorithm, loading protocols were designed to generate high-cycle fatigue cracks in *C(T)* specimens that are similar to those one would see in full-scale steel bridges subject to traffic loading. The objective is to limit the plastic deformation at the crack tip throughout the fatigue testing. Finally, the hypothesis, and the proposed algorithm, were experimentally evaluated using steel *C(T)* specimens instrumented with SECs for a series of high-cycle fatigue tests to examine whether crack growth could be successfully monitored based on the proposed approach.

2. Background

The SEC is a flexible capacitor formed by a dielectric layer sandwiched between to conductive layers acting as electrodes. The dielectric is composed of a styrene-ethylene/butylene-styrene (SEBS) block co-polymer filled with titania, and the conductive layers are fabricated by the same SEBS, filled with carbon black (Figure 1b). The SEC is attached onto the surface to be monitored, typically using off-the-shelf bi-component epoxy. Strain produces a geometric change in the sensor, producing a corresponding change in capacitance. (Figure 1a). SECs can be fabricated in various sizes. A dimension of 76 mm by 76 mm (3 in by 3 in) was adopted in this study. The effective sensing area, or the area of the conductive layer, is 63.5 mm by 63.5 mm (2.5 in by 2.5 in). Figure 1c shows a picture of one SEC with two strips of copper tape embedded in the top and bottom

conductive plates for connecting to the data acquisition (DAQ). A detailed description about the fabrication procedure of the sensor can be found in reference [16].

As illustrated in Figure 1b, when the monitored structures is under a tensile (or compressive) force, the surface strain provokes a change in the SEC's area A and thickness h, leading to a change ΔC in capacitance C. Starting with the approximation of the SEC as a pure capacitor

$$C = \frac{e_0 e_r A}{h} \tag{1}$$

where e_0 is the permittivity of air, e_r is the permittivity of the dielectric, $A = w \cdot l$ is the sensing area of width w and length l, and h is the thickness of the dielectric. It can be shown that, under uniaxial strain ε, the change in capacitance is given by [26]:

$$\frac{\Delta C}{C} = \frac{1}{1-\nu}\varepsilon \tag{2}$$

where ν is the SEC's Poisson ratio (ν approx. 0.49, with 1/(1-ν) approx. 2).

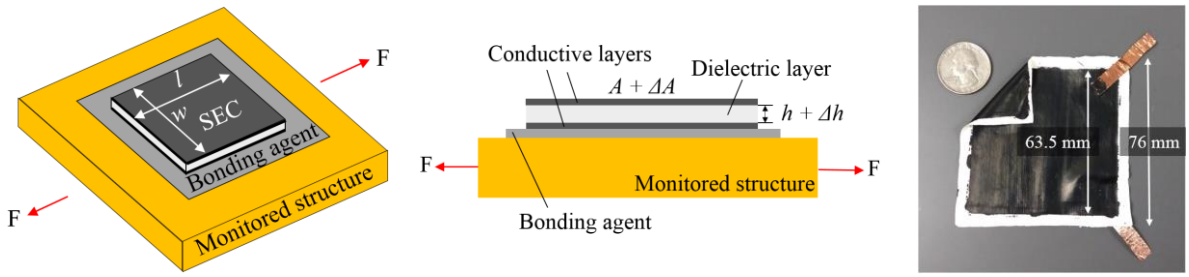

(a) (b) (c)

Figure 1. (a) Schematic of the SEC; (b) the SEC under a tensile strain; and (c) a picture of the SEC

The authors approached this investigation with a hypothesis that the strain sensing ability of the SEC could be extended to fit the purpose of fatigue crack monitoring in steel bridges. Figure 2 demonstrates a supporting principle using a steel plate as an example. The fatigue load F is assumed to have a constant load range, and a fatigue crack initiates at the left edge of the plate and propagates to the right. The SEC is deployed on the plate prior to the crack initiation. Points a, b, and c represent three stages of crack propagation when the crack tip first reaches these locations.

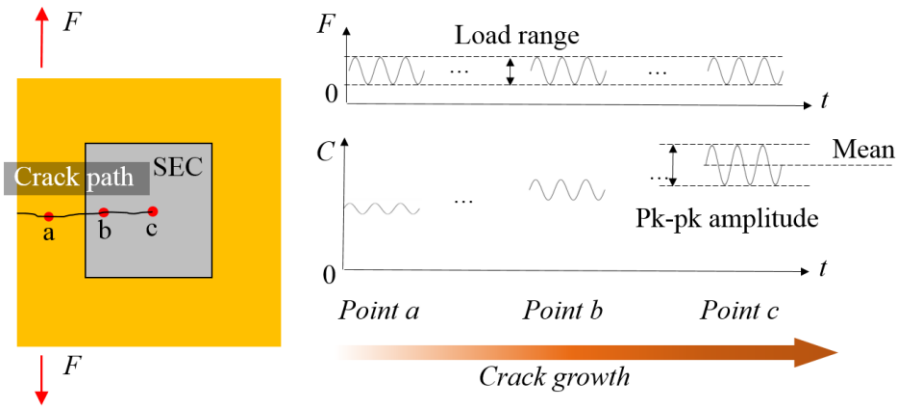

Figure 2. Schematic of the sensing principle for crack monitoring

The crack monitoring capabilities of the SEC can conceptually be thought of as occurring across three stages of crack growth:

1) When the crack is approaching the SEC (point *a*), the sensor can be treated as a large area strain gage, where localized strain changes can be measured by a change in capacitance *C*;

2) When the crack grows into the sensing area (point *b*), the crack opening beneath the sensing skin produces a stretch in the SEC, and thus causes an additional increase in capacitance. Therefore, larger responses in terms of both the mean and the pk-pk amplitude should be observable;

3) When the crack propagates further (point *c*), higher responses for both mean capacitance and pk-pk amplitude should be measurable. This is due to the fact that the crack weakens the local stiffness of the plate (i.e. the crack opens more under same range of the load).

A challenge associated with SECs is that measurements can be subject to capacitance drift [31] during long-term monitoring due to environmental factors such as temperature or humidity changes, and to an intrinsic electrical behavior found in many sensors fabricated from smart materials [32, 33].

To ensure robustness against capacitance drift, the pk-pk amplitude of the capacitance measurement (as illustrated in Figure 2) was hypothesized to be an indicator of cracking useful for long-term monitoring of fatigue cracking. By extracting only the pk-pk amplitude, the drift effect in the mean capacitance can be filtered out. To illustrate, denote $C_{pk\text{-}pk}$ as the pk-pk amplitude of the sensor's capacitance. $C_{pk\text{-}pk}/C_m$ is then the percentage change of capacitance of the SEC reflecting the amount of strain transmitted to the SEC, where C_m is the mean capacitance. Using the sensing principle (Equation 2):

$$\frac{C_{pkpk}}{C_m} = 2\varepsilon \tag{3}$$

Now, assume that the excitation load range ΔF is constant over the long-term period, but that the capacitance drifts by ΔC_m, as illustrated in Figure 3. Such a drift would provoke a change to the pk-pk amplitude ΔC_{pkpk} as well. Since the monitored strain remains constant before and after the drift, the corresponding relative change in capacitance should remain the same:

$$\frac{C_{pkpk}}{C_m} = \frac{C_{pkpk} + \Delta C_{pkpk}}{C_m + \Delta C_m} = 2\varepsilon \tag{4}$$

Rearranging Equation 4 provides:

$$\frac{\Delta C_{pkpk}}{C_{pkpk}} = \frac{\Delta C_m}{C_m} \tag{5}$$

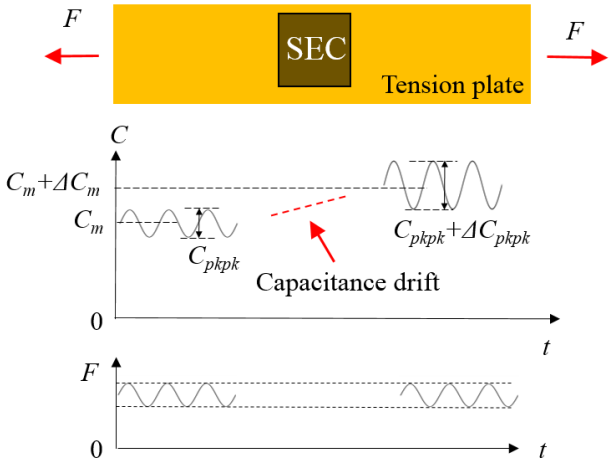

Figure 3. Illustration of drift impact on both mean and pk-pk amplitude of capacitance measurement

Equation 5 indicates that the percentage change of the pk-pk amplitude caused by the capacitance drift $\Delta C_{pkpk}/C_{pkpk}$ is the same as the percentage change of the mean capacitance $\Delta C_m/C_m$. In the fatigue tests of this study, a maximum capacitance drift was found as 10 pF during a period of several weeks, leading to $\Delta C_{pkpk}/C_{pkpk} = \Delta C_m/C_m$ = 10 pF / 900 pF = 1.1 %, in which the 900 pF is a typical mean capacitance C_m of the SECs. On the other hand, test results in this study also showed that $\Delta C_{pkpk}/C_{pkpk}$ caused by crack growth reached 100% when the crack grows from 0 mm (0 in.) to 46.0 mm (29/16 in.). Such an increment provoked by the crack growth (100%) is much larger than the change of capacitance drift (1.1%) so that the drift can be neglected for tests in this study.

The pk-pk amplitude is sensitive to signal-to-noise ratio due to its small magnitude. For high-cycle fatigue cracks, the pk-pk amplitude can even be smaller, given that fatigue in steel bridges is usually driven by relatively low stress ranges. To robustly and accurately identify pk-pk amplitude, a crack monitoring algorithm is proposed based on frequency analysis, as explained in the next section.

3. Crack Monitoring Algorithm for High-cycle Fatigue Cracks

An illustration of SEC application for crack monitoring in steel bridges is shown in Figure 4. Fatigue cracks can take years to decades to initiate and propagate before reaching a critical size [3]. For this reason, continuously collecting data throughout bridge service life is impractical. An effective crack monitoring strategy would follow a multi-timescale [34]: a fast timescale for data collection and a slow timescale for tracking crack growth. As shown in Figure 4, in the fast timescale monitoring, a short-time measurement is taken by the SEC network. Within the period of measurement, the fatigue crack can be assumed unchanged. An indicator of crack length can be extracted for this particular point-in-time using a crack monitoring algorithm. By taking multiple fast timescale measurements and extracting features of crack length over the slow-timescale over the entire fatigue life, the global behavior of crack growth can be identified.

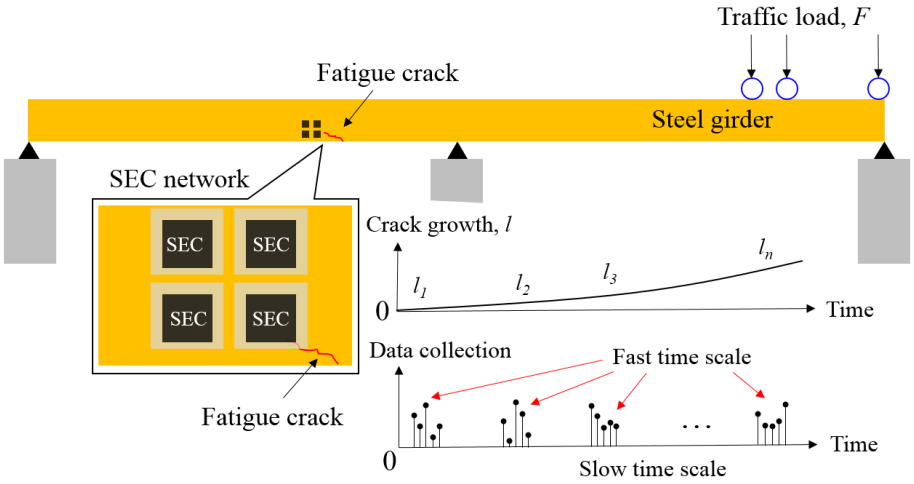

Figure 4. Demonstration of fatigue crack monitoring in steel bridges using SEC network

For this approach to be viable, a computed value is required to serve as an indicator of crack length; the Crack Growth Index (*CGI*) was developed to serve as such an indicator.

The *CGI* acts as a normalized strain indicator from which crack growth under the SEC can be inferred. Figure 5 depicts the steps used in the developed crack monitoring algorithm for extracting the *CGI*. The algorithm is a four-step procedure including data acquisition, frequency analysis, establishing *CGIs*, and crack growth monitoring.

The first step in the monitoring algorithm is data acquisition (Figure 5a). A series of short time measurements are taken as the crack grows to different lengths (l_i). Both capacitance measurements $C_i(t)$ of the SEC and force measurements $F_i(t)$ of the fatigue load are collected. The pk-pk amplitude of the SEC is directly related to the opening of the crack, but is also affected by the magnitude of load. To successfully identify crack growth through the SEC's response, the capacitance measurements $C_i(t)$ should be normalized with respect to the level of fatigue load. The fatigue load can either be directly measured or indirectly determined via strain measurements.

The next step in the monitoring algorithm is to convert the capacitance, $C_i(t)$, and force measurements, $F_i(t)$, from the time domain to Power Spectral Densities (PSDs) in the frequency domain. Physically, a PSD represents the energy distribution of a signal in the frequency domain. The peak amplitude is then identified to represent the pk-pk amplitude of the time series. Compared with identifying the pk-pk amplitude in the time domain, the peak of the PSD in the frequency domain is less sensitive to noise content in the measurements. As shown in Figure 5b, $peak_i^F$ is denoted as the PSD peak of the i^{th} force measurement $F_i(t)$, and $peak_i^C$ as the PSD peak of the i^{th} sensor measurement $C_i(t)$. Both $peak_i^F$ and $peak_i^C$ should locate at the same frequency (i.e. the loading frequency), but may have different amplitudes.

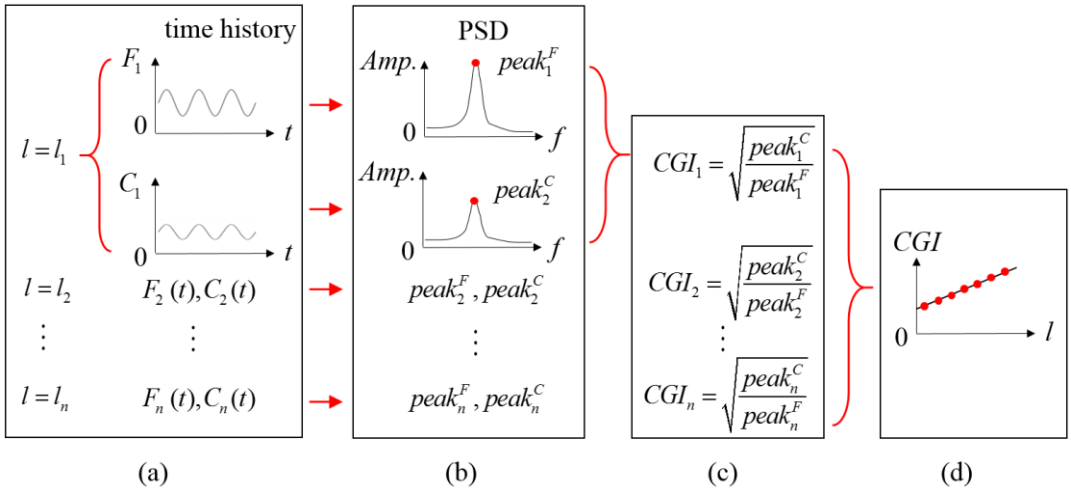

Figure 5. The four-steps involved in the proposed crack monitoring algorithm: (a) data acquisition; (b) frequency analysis; (c) establishing *CGIs*; and (d) crack growth monitoring

Once the PSD peaks are obtained, *CGIs* can be computed using equations shown in Figure 5c. *CGI* is a feature extracted from sensor's measurement $C_i(t)$ and applied load $F_i(t)$. It represents the level of the pk-pk amplitude under a unit excitation load.

In the final step of the algorithm, crack growth is monitored using the *CGI* values. Specifically, CGI_i at the i^{th} measurement is correlated with its crack length l_i, so that a curve between *CGI* and crack length can be established (Figure 5d).

Fatigue testing was performed as part of this study to evaluate to what extent crack growth can be indicated by monitoring increasing *CGI*, and to evaluate the overall effectiveness of the monitoring algorithm.

4 Fatigue Loading Protocols

In previous investigations focused on the SEC performance in the presence of low-cycle fatigue cracks [26, 27, 28], a fatigue load with a 26.0 kN (5.85 kip) constant range was applied to specimens. However, a constant load range only guarantees relatively small crack openings in the early stages of crack propagation. As the crack grows longer, excessive opening and plastic deformation at the crack tip can occur due to significant stiffness reduction. This leads to crack characteristics which are not representative of fatigue cracks that commonly occur in steel bridges.

To generate realistic high-cycle fatigue cracking, the loading protocol used in this study was based on maintaining a constant range of applied stress intensity, ΔK. A relatively low value for ΔK was used to limit formation of a large plastic zone at the crack tip so that crack openings remained small even as the crack length increased. This approach generated fatigue cracks that are more representative in steel bridges. ΔK is the range of stress intensity within one load cycle and can be expressed as:

$$\Delta K = K_{max} - K_{min} \tag{5}$$

where K_{max} and K_{min} are the maximum and minimum stress intensity factors. In fracture mechanics, ΔK is a parameter representing the stress state change around the crack tip caused by the fatigue load ΔF. According to ASTM E1820-15 [35], for the compact tension specimen adopted in this study (Figure 6), ΔK can be determined as:

$$\Delta K = \frac{\Delta F}{B\sqrt{W}} f(\frac{a}{W}) \tag{6}$$

where $\Delta F = F_{max} - F_{min}$ is the difference between the maximum load F_{max} and the minimum load F_{min} in one load cycle; B is the thickness of the specimen; a is the length of the crack measured from the load line; and W is the distance between load line and the back face of the specimen. The term $f(a/W)$ in Equation 6 is a polynomial with the variable a/W. Detailed expressions for $f(a/W)$ can be found in reference [35]. Dimensions a and W are also labeled in the schematic presented in Figure 6.

From Equation 6, ΔF can be determined once a desired ΔK is established, but this requires knowledge of F_{max} and F_{min}. A common approach is to introduce the stress ratio, $R = K_{min} / K_{max} = F_{min} / F_{max}$, representing the ratio of maximum stress and minimum stress in one load cycle. In the case of steel bridges, R is the ratio between the magnitude of live load-induced stress (i.e. vehicle load) and the magnitude of dead load-induced stress (i.e. bridge self-weight), at a particular location on the structure.

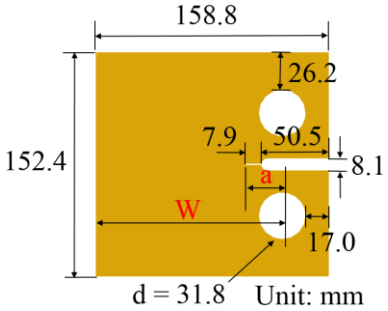

Figure 6. Dimensions of the *C(T)* specimen;

The procedure used to apply the loading protocol is summarized in Figure 7. A constant ΔK was first assigned. Then, based on ASTM E1820 [35], the corresponding ΔF for the targeted ΔK was computed. Finally, a chosen magnitude for the stress ratio R guarantees a unique solution of F_{max} and F_{min}, so that the loading protocol can be applied using load control. Three R values were used in the test program: 0.1, 0.4, and 0.6, simulating stress ratios caused by passing vehicles with different weights in steel bridges.

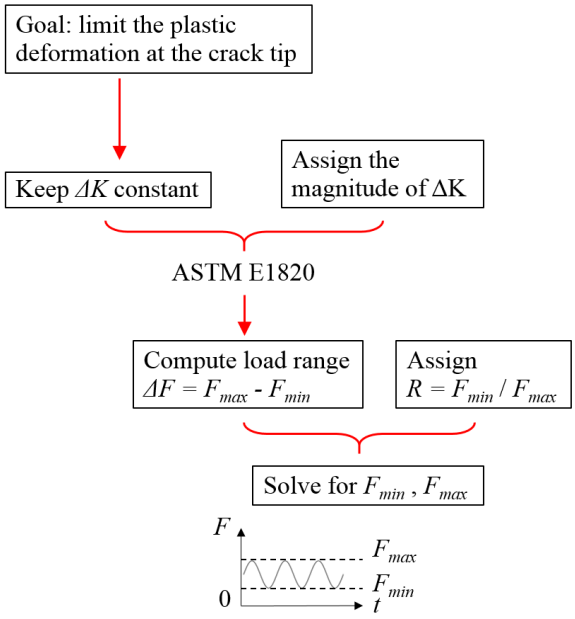

Figure 7. Procedure for determination of the fatigue loading protocol

5 Experimental Validations

The SEC's ability to monitor high-cycle fatigue cracks was investigated through fatigue testing performed on steel *C(T)* specimens. The suitability of the monitoring algorithm was evaluated based on the experimental findings.

5.1 Test configuration

A series of small-scale steel specimens equipped with SECs were tested under fatigue loading using a constant ΔK. *C(T)* specimens were fabricated from A36 steel plates of 6.4 mm (1/4 in.) thickness. Figure 6 shows the dimensions of the *C(T)* specimen. The specimens were loaded using a closed-loop servo-hydraulic uniaxial load frame utilizing two clevises. Two adhesive measuring tapes were adhered to the front face of each specimen (Figure 8a) to allow for visual measurement of crack length during testing. The SEC was attached to the back face of the specimen using bi-component epoxy JB-Weld (Figure 8b), while the top and bottom conductive layers of the SEC were connected to a DAQ system (ACAM PCAP02) for measuring the capacitance response.

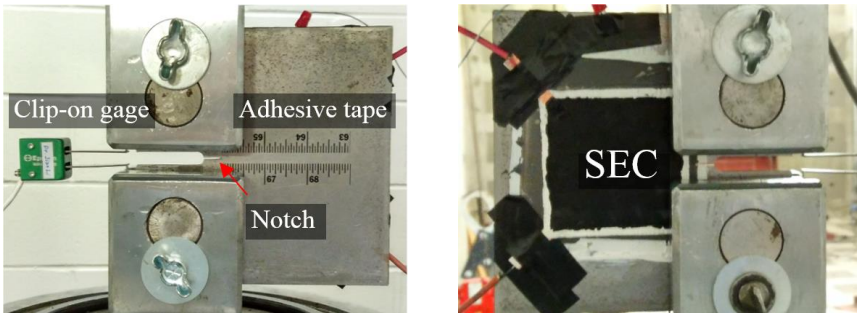

(a) (b)

Figure 8. (a) Front face of the specimen; and (b) back face of the specimen

Table 1 summarizes the experimental testing procedures used on the three tests included as part of this study, as well as the previous low-cycle fatigue test [28]. Test 1 was performed using R=0.1. Tests 2 and 3 were performed with identical test parameters, using R=0.6 during crack propagation, but R=0.4 and R=0.6 during each data collection interval. This was done to enhance an understanding of the influence of the stress ratio on SEC performance.

Table 1. An overview of the procedure on experimental testing

Test number	Range of stress intensity factor ΔK	Crack propagation stage	Data collection stage
Test 1	22.0 to 27.5 $MPa\sqrt{m}$ (20 to 25 $ksi\sqrt{in.}$)	R = 0.1	Figure 9, R = 0.1
Test 2 and Test 3	22 $MPa\sqrt{m}$ (20 $ksi\sqrt{in.}$)	R = 0.6	Figure 9, R = 0.4 Figure 9, R = 0.6
Previous Low-cycle Fatigue Test [28]	48.3 to 146.7 $MPa\sqrt{m}$ (44.5 to 133.5 $ksi\sqrt{in.}$)	R = 0.1	Figure 9, R = 0.1

A loading frequency of 10 Hz was used for initiating and propagating fatigue cracks. Data collection was performed at every 1.6 mm (1/16 in.) increment of crack growth, and the loading rate was reduced to 0.5 Hz while data was being collected. For each data collection interval, data were sampled at 50 Hz over 100 cycles, and measurements were recorded for actuator force and capacitance of the SEC. After each data collection interval, the fatigue loading rate was returned to 10 Hz so that the crack propagation could be continued.

Figure 9 presents the loading protocols applied in the tests with different R ratios: 0.1 (Test 1), 0.4 (Tests 2 and 3), and 0.6 (Tests 2 and 3). The loading protocol used by [28] for low-cycle fatigue testing is also shown for comparison. It can be seen that the ΔK values used in Tests 1, 2, and 3 were much smaller than used in [28], representing a higher demanding on the SEC's resolution. Note that crack lengths in these plots were measured from the notch of the specimen (Figure 8a).

The relationship between stress intensity factor, applied stress, and crack length defined in Equation 6 indicates that a longer crack length, a, should correspond to a smaller ΔF if the target ΔK is fixed. This relationship mandates that the difference between the minimum and maximum

bounds of the fatigue loading should decrease as the crack grows. As shown in Figure 9a, a multi-stage loading protocol was adopted in Test 1, in which ΔF was re-computed and adjusted for every 9.5mm (3/8 in.) of crack propagation, maintaining an approximately constant ΔK within a range between 22.0 $MPa\sqrt{m}$ to 27.5 $MPa\sqrt{m}$ (20 $ksi\sqrt{in.}$ to 25 $ksi\sqrt{in.}$). In Tests 2 and 3, shown in Figure 9b and c, more frequent adjustments were made by decreasing ΔF every 1.6 mm (1/16 in.) of crack growth. This ensured that ΔK was maintained at 22.0 $MPa\sqrt{m}$ (20 $ksi\sqrt{in.}$) throughout Tests 2 and 3.

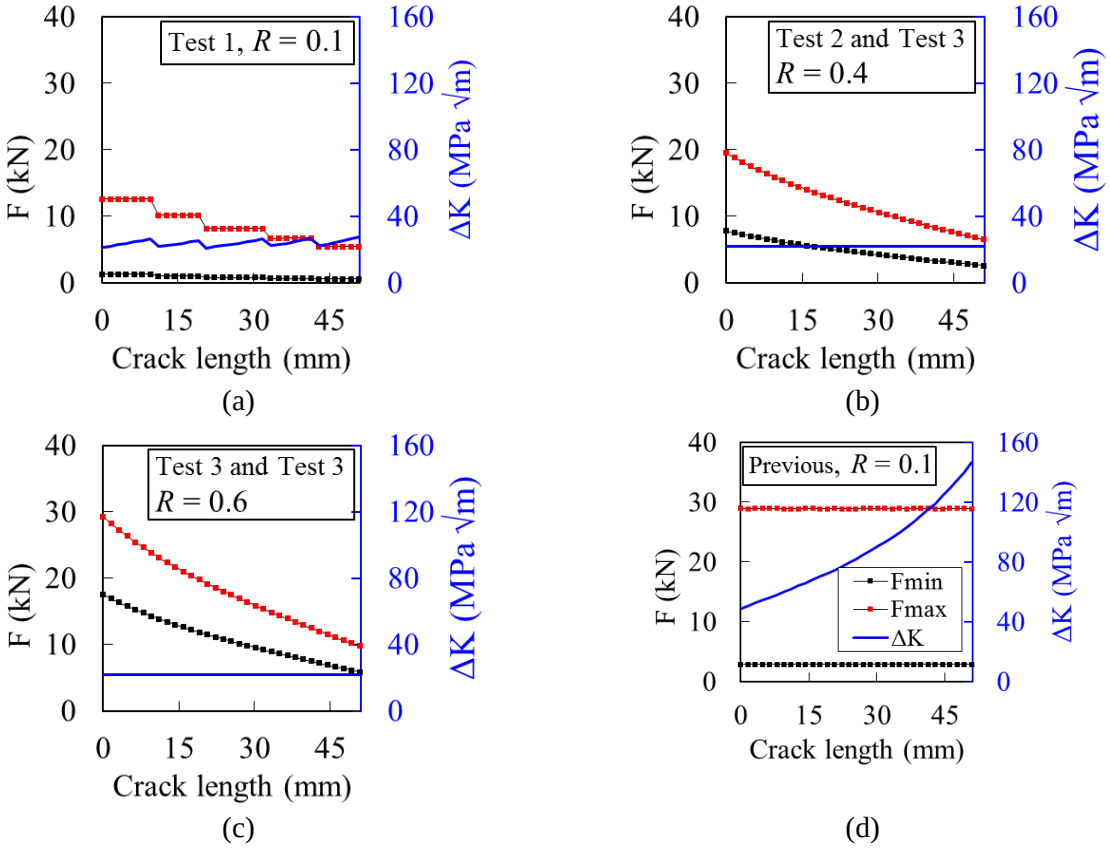

Figure 9. (a) Test 1 loading protocol, R = 0.1; (b) Test 2 and 3 loading protocol, R = 0.4; (c) Test 2 and 3 loading protocol, R = 0.6; and (d) Loading protocol used in prior low-cycle fatigue test [28], R = 0.1. Red dotted line represents F_{max}, black dotted line represents F_{min}, and blue line represents ΔK.

5.2 Crack growth under the new loading protocols

Figure 10 presents a comparison between cracking generated by maintaining an approximately constant value for ΔK, and that generated in previous testing by maintaining a constant value for ΔF. Although the crack sizes obtained in Tests 1 is significantly longer than that observed during the previous low-cycle fatigue testing, crack opening was observed to be much smaller. Due to the large crack opening in the previous test, excessive plastic deformation produced a dimple which

could be observed at the crack tip, while such plastic deformation was not observed in the tests performed as part of the current study.

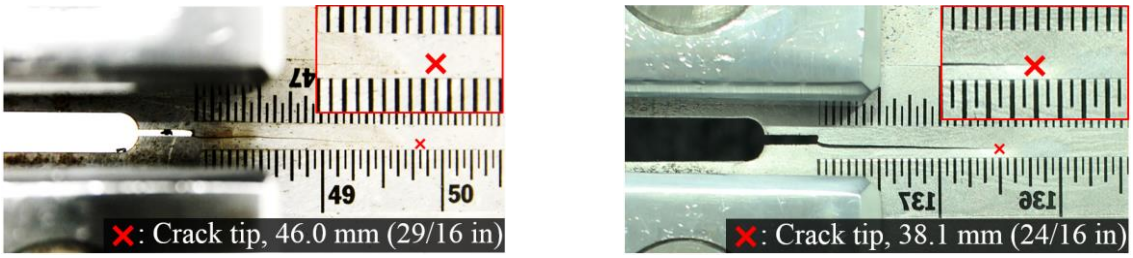

(a) (b)

Figure 10. Pictures of cracks showing different features between the new and previous tests: (a) crack in Test 1 at 46.0 mm (29/16 in.); and (b) crack from previous testing [27] at 38.1 mm (24/16 in.)

Table 2 summarizes the fatigue test results, and includes the number of cycles applied, final crack length, and fracture status. Because the load range was continuously decreased in Tests 1, 2, and 3, these specimens did not experience fracture. In the previous test, the specimen failed in ductile tearing when the crack reached a length of 37.1 mm (24/16 in.). Tests 1, 2, and 3 produced significantly longer fatigue lives than noted in the specimen previously tested because of the lower ΔK. In particular, nearly 2 million cycles were applied in Test 1, which was performed at the lowest stress ratio (R = 0.1).

Table 2. Fatigue testing results

Test number	Number of cycles	Final crack length	Specimen fracture
Test 1	1,810,000	46.0 mm (29/16 in.)	No
Test 2	660,000	50.8 mm (32/16 in.)	No
Test 3	605,000	50.8 mm (32/16 in.)	No
Previous Low-cycle Fatigue Test [28]	14,500	37.1 mm (24/16 in.)	Yes

5.3 Evaluation of proposed crack monitoring algorithm

Figure 11 presents sample raw capacitance measurements from the SECs in Tests 1, 2, and 3 as cracking propagated in the *C(T)* specimens. Full detailed SEC measurements of Test 1 are demonstrated in reference [36]. For better pk-pk amplitude comparisons, all the measurements have been detrended to have a zero mean. Results in these figures show an increasing trend of pk-pk amplitudes as cracking propagated. For example, the pk-pk amplitude increased from approximately 0.5 pF to 2 pF when the crack grew from 0 mm (0 in.) to 46.0 mm (29/16 in.). The SEC's measurements showed similar levels of response among the tests for similar crack lengths. One example is that pk-pk amplitudes were approximately 2 pF for all three tests (and all three R values tested) when the crack reached 46.0 mm (29/16 in.), as shown in the last column of the

figures. This finding indicates that for a certain crack length, sensor response is governed by load range ΔF and is invariant to stress intensity ratio R.

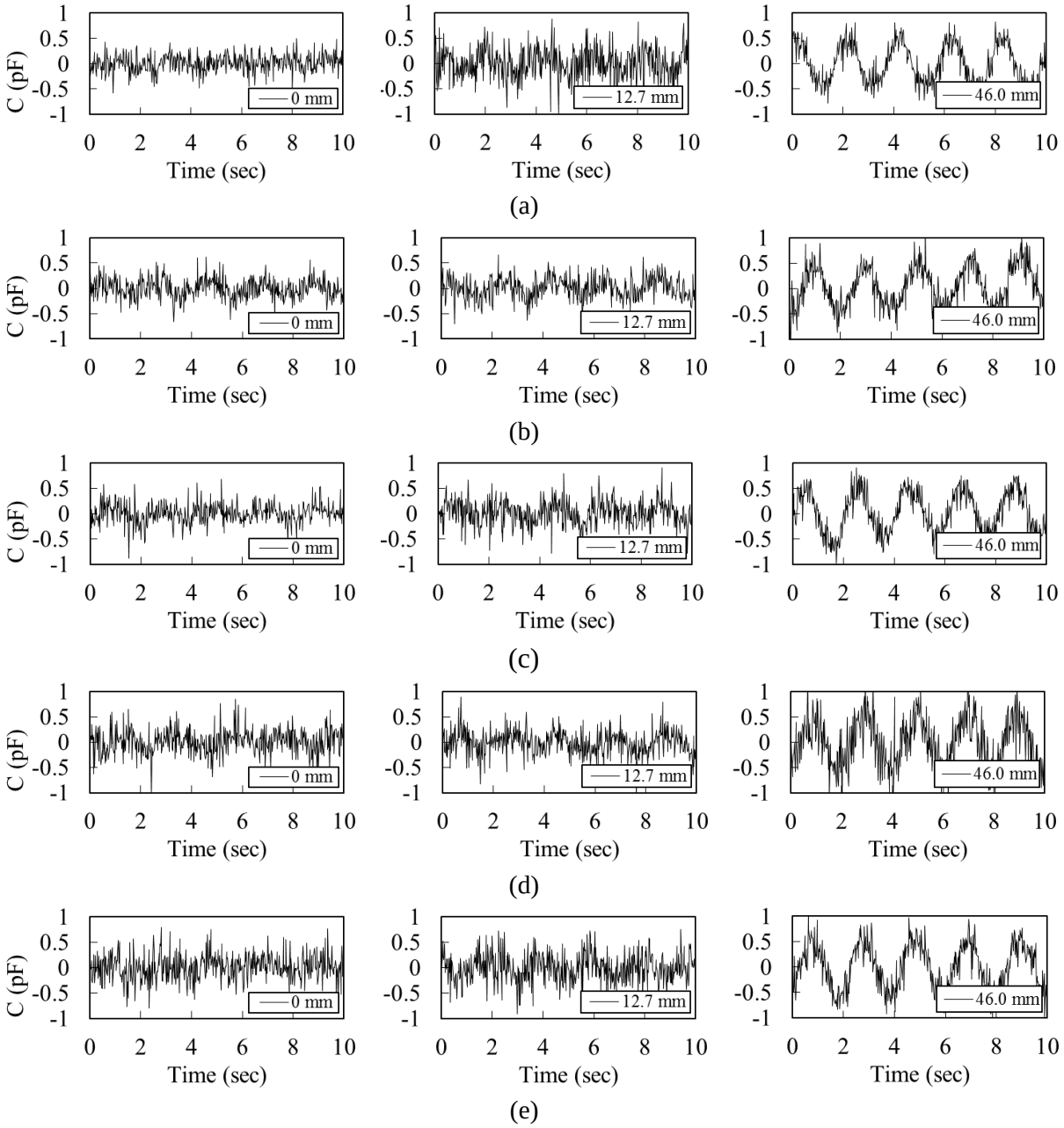

Figure 11. Sample raw measurements of SECs when the crack propagates to different lengths: (a) Test 1, R = 0.1; (b) Test 2, R = 0.4; (c) Test 2, R = 0.6; (d) Test 3, R = 0.4; and (e) Test 3, R = 0.6. The crack lengths are indicated in each plot.

Figure 11 also exhibits noise content in the capacitance measurements, especially when crack lengths were short. Identifying the pk-pk amplitudes directly from the raw measurements in the time domain will suffer from uncertainty due to this noise content. For this reason, the proposed crack monitoring algorithm based on frequency analysis was utilized.

Figure 12 shows the outcome of the crack monitoring algorithm for all testing cases. The plot for Test 1 is missing data for some crack lengths. This is due to faster than anticipated crack growth. In subsequent tests, more frequent observations were scheduled in order to avoid this loss of data.

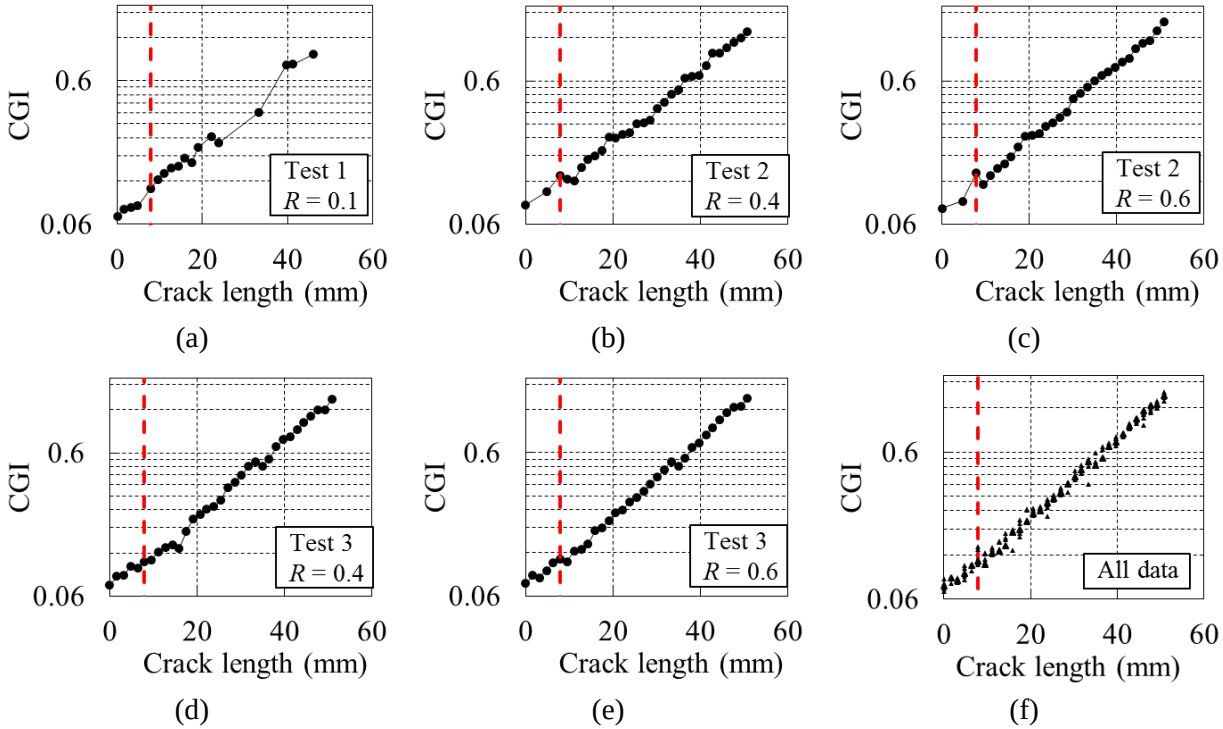

Figure 12. Representative measurements of SECs as the crack propagated to different lengths: (a) Test 1; (b) Test 2, R = 0.4; (c) Test 2, R = 0.6; (d) Test 3, R = 0.4; (e) Test 3, R = 0.6; and (f) a comparison of all data. Red dashed line indicates the start of effective sensing area on the SEC.

The crack length in Figure 12 is measured from the notch of the specimen (Figure 8a). However, due to the fact that the effective sensing area of the SEC is less than its outermost dimensions, the crack does not reach the effective sensing area when it initiates from the notch. As shown in Figure 13, the notch is at a distance of 7.9 mm (5/16 in.) from the edge of the sensing area. The dashed red line in Figure 12 indicates the start of the SEC's effective sensing area.

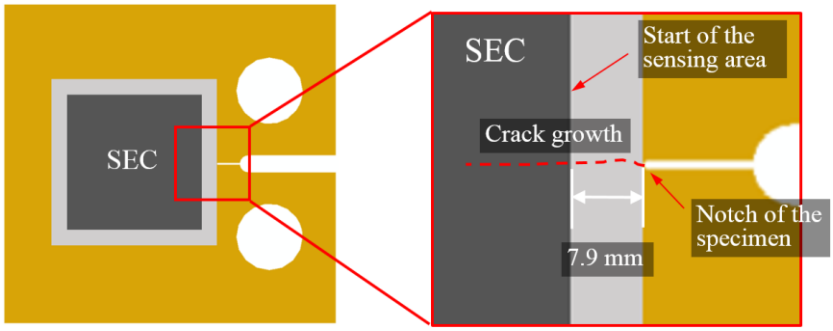

Figure 13. Demonstration of the boundary of the sensing area

A positive correlation between *CGI* and crack length can be clearly observed in Figure 12a-e. An approximate linear relationship was identified between crack length and log(*CGI*). The data shows

that fatigue crack growth can be successfully identified by monitoring the *CGI* values produced based on the developed algorithm. Furthermore, such a trend also exists when the crack is approaching, but has not quite reached the sensing area, as shown by the data points prior to the red dashed line. This is because the SEC essentially acts as a large-area strain gauge for monitoring the increasing strain field cause by crack growth. As a crack monitoring method based on direct strain measurement, its effectiveness is validated when the crack is either close to or directly underneath the SEC.

Figure 12f shows a compilation of *CGIs* for Tests 1, 2, and 3. Excellent agreement was observed between all tests in which fatigue loading with different stress intensity ratios were applied. Considering the fact that a bridge under traffic loading is subject to changing stress intensity ratios over time, the result in this plot indicate the SEC could robustly monitor high-cycle fatigue cracks under different stress ratios, *R*.

Based on the finding, the proposed crack monitoring algorithm provided a good solution for monitoring fatigue crack growth using an SEC. The algorithm showed robustness even when the crack was small and the measurements were contaminated by noise content. Moreover, the proposed algorithm proved to be applicable for various loading conditions.

6. Conclusions and Future Work

This paper has presented a study that was focused on examining the suitability of a novel large-area strain-based sensing technology for monitoring fatigue cracking in steel bridges. The SEC is a large-size, flexible, low-cost, and mechanically-robust capacitive strain gage, and has a wide strain measuring range, making it a promising tool for monitoring cracking in bridges. Previous studies have verified the SEC's capabilities for monitoring low-cycle fatigue cracking, but high-cycle fatigue cracking is characterized by small crack openings, which presents a new challenge for a capacitance-based sensor such as the SEC. To achieve a monitoring solution for fatigue cracking in steel bridges, the pk-pk amplitude of the sensor's measurement was used to construct an indicator of crack growth. Then, a crack monitoring algorithm was established to compute *CGIs* as a normalized pk-pk amplitude in frequency domain. The sensor's capabilities and the proposed algorithm were evaluated through experimental testing under various stress ratios, *R*. The following conclusions were drawn:

- The developed algorithm was able to overcome noise infiltration, and resulted in excellent correlation between increasing fatigue crack length and increasing *CGI*. Therefore, the proposed crack monitoring algorithm was validated by the test data.
- The proposed crack monitoring algorithm was able to robustly monitor the growth of high-cycle fatigue cracks under various loading conditions, and provided consistent results for the three stress ratios that were studied.
- With the introduction of the monitoring algorithm, the SEC was found to be capable of serving as a monitoring device for propagating fatigue cracks in steel bridges.

This study was focused on the SEC's capability to monitor in-plane fatigue cracks, and the linear relationship between log (*CGI*) and crack length is dependent on the size of SECs. Future work will be focused on testing the SEC in larger scale structural models with more complex geometric layouts for out-of-plane distortion-induced fatigue cracks in bridge components.

Additionally, the fatigue load in this study was assumed to be a periodic sinusoidal wave with a single dominant frequency. Fatigue cracks in steel bridges are generated by traffic loads. Depending on the weight and speed of passing vehicle, traffic load may contain more complex features like different pk-pk amplitudes and frequency components. Our future work will focus on updating the current crack monitoring algorithm for steel bridge applications under complex traffic loads.

The research reported in this paper forms the basis for use of SECs as a robust fatigue monitoring solution in steel bridges. Development of such a monitoring solution is highly impactful, as the sensors themselves are large and can cover large areas in fatigue-susceptible regions of steel bridges, leading to more reliable and comprehensive long-term fatigue monitoring solutions.

ACKNOWLEDGEMENTS

This work was supported by Transportation Pooled Fund Study TPF-5(328), which includes the following participating state DOTs: Kansas, Iowa, Minnesota, North Carolina, Pennsylvania, Texas, and Oklahoma; and Iowa Department of Transportation grant #RT454-494. Their support is gratefully acknowledged. The authors also want to thank undergraduate assistant Duncan MacLachlan and visiting PhD student Jie Wu for assisting with fatigue testing at the University of Kansas, and Austin Downey from Iowa State University for providing support regarding the data acquisition system.

REFERENCES

[1] Haghani, R., Al-Emrani, M., & Heshmati, M. (2012). Fatigue-prone details in steel bridges. *Buildings*, **2**(4), 456-476.

[2] Phares, B. M., Rolander, D. D., Graybeal, B. A., & Washer, G. A. (2001). Reliability of visual bridge inspection. *Public Roads*, **64**(5).

[3] Zhao Z, and Haldar A. (1996). Bridge fatigue damage evaluation and updating using non-destructive inspections. *Engineering fracture mechanics*. **53**(5), 775-88

[4] Roberts, T., & Talebzadeh, M. (2003). Acoustic emission monitoring of fatigue crack propagation. *Journal of Constructional Steel Research*, **59**(6), 695-712.

[5] Ihn JB, and Chang FK. (2004). Detection and monitoring of hidden fatigue crack growth using a built-in piezoelectric sensor/actuator network: I. Diagnostics. *Smart materials and structures*. **13**: 609

[6] Staszewski, W. J., Lee, B. C., & Traynor, R. (2007). Fatigue crack detection in metallic structures with Lamb waves and 3D laser vibrometry. *Measurement Science and Technology*, **18**(3), 727.

[7] Blunt, D. M., & Keller, J. A. (2006). Detection of a fatigue crack in a UH-60A planet gear carrier using vibration analysis. *Mechanical Systems and Signal Processing*, **20**(8), 2095-2111.

[8] Yeum CM, and Dyke SJ. (2015). Vision‐Based Automated Crack Detection for Bridge Inspection. *Computer-Aided Civil and Infrastructure Engineering*. **30**(10), 759-70

[9] Jahanshahi, M. R., & Masri, S. F. (2013). A new methodology for non-contact accurate crack width measurement through photogrammetry for automated structural safety evaluation. *Smart materials and structures*, **22**(3), 035019.

[10] Adhikari RS, Moselhi O, and Bagchi A. (2014). Image-based retrieval of concrete crack properties for bridge inspection *Automation in construction*. **39** 180-94

[11] Yao Y, Tung ST, and Glisic B. (2014). Crack detection and characterization techniques—An overview *Structural Control and Health Monitoring*. **21**(12), 1387-413

[12] Tikka J, Hedman R, and Silijander A. (2003, September). Strain gauge capabilities in crack detection *4th International Workshop on Structural Health Monitoring.* 15-17

[13] Glisic B, and Inaudi D. (2011). Development of method for in-service crack detection based on distributed fiber optic sensors. *Structural Health Monitoring.* **11**(2), 161-171.

[14] Loh KJ, Lynch JP, Shim BS, and Kotov NA. (2008). Tailoring piezoresistive sensitivity of multilayer carbon nanotube composite strain sensors *Journal of Intelligent Material Systems and Structures.* **19**(7), 747-64

[15] Dai H, Thostenson ET, and Schumacher T. (2015). Processing and Characterization of a Novel Distributed Strain Sensor Using Carbon Nanotube-Based Nonwoven Composites *Sensors*. **15**(7), 17728-47

[16] Yao Y, and Glisic B. (2015). Detection of steel fatigue cracks with strain sensing sheets based on large area electronics *Sensors*. **15**(4), 8088-108

[17] Loh KJ, Kim J, Lynch JP, Kam NW, and Kotov NA. (2007). Multifunctional layer-by-layer carbon nanotube–polyelectrolyte thin films for strain and corrosion sensing *Smart Materials and Structures*. **16**(2), 429.

[18] Mohammad I, and Huang H. (2010). Monitoring fatigue crack growth and opening using antenna sensors *Smart Materials and Structures*. **19**(5), 055023

[19] Yi X, Cho C, Cooper J, Wang Y, Tentzeris MM, and Leon RT. (2013). Passive wireless antenna sensor for strain and crack sensing - electromagnetic modeling, simulation, and testing *Smart Materials and Structures*. **22**(8), 085009

[20] Laflamme S, Ubertini F, Saleem H, D'Alessandro A, Downey A, Ceylan H, and Materazzi AL. (2014). Dynamic characterization of a soft elastomeric capacitor for structural health monitoring *Journal of Structural Engineering*. **141** 04014186

[21] Laflamme S, Kollosche M, Connor JJ, and Kofod G. (2012). Robust flexible capacitive surface sensor for structural health monitoring applications *Journal of Engineering Mechanics*. **139** 879-85.

[22] Laflamme S, Saleem HS, Vasan BK, Geiger RL, Chen D, Kessler MR, and Rajan K. (2013). Soft elastomeric capacitor network for strain sensing over large surfaces *IEEE/ASME Transactions on Mechatronics*. **18** 1647-54

[23] Laflamme, S., Kollosche, M., Connor, J. J., & Kofod, G. (2012). Robust flexible capacitive surface sensor for structural health monitoring applications. *Journal of Engineering Mechanics*, **139**(7), 879-885.

[24] Saleem H, Downey A, Laflamme S, Kollosche M, and Ubertini F. (2015). Investigation of Dynamic Properties of a Novel Capacitive-based Sensing Skin for Nondestructive Testing *Materials Evaluation*. **73** 1384-91

[25] Downey, A., Laflamme, S., & Ubertini, F. (2016). Reconstruction of in-plane strain maps using hybrid dense sensor network composed of sensing skin. *Measurement Science and Technology*, **27**(12), 124016.

[26] Kharroub S, Laflamme S, Song C, Qiao D, Phares B, and Li J. (2015). Smart sensing skin for detection and localization of fatigue cracks *Smart Materials and Structures*. **24** 065004

[27] Kong X, Li J, Laflamme S, and Bennett C. (2015). Fatigue Crack Monitoring using Large-area, Flexible Capacitive Strain Sensors. *The 6th International Conference on Advances in Experimental Structural Engineering (6AESE) and 11th International Workshop on Advanced Smart Materials and Smart Structures Technology (11ANCRiSST).* University of Illinois at Urbana-Champaign

[28] Kong X, Li J, Bennett C, Collins W, and Laflamme S. (2016). Model calibration for a soft elastomeric capacitor sensor considering slippage under fatigue cracks. *SPIE Smart Structures* and Materials + Nondestructive Evaluation and Health Monitoring International Society for Optics and Photonics pp.98032P

[29] Kong, X., Li, J., Laflamme, S., Bennett, C., & Matamoros, A. (2015, April). Characterization of a soft elastomeric capacitive strain sensor for fatigue crack monitoring. *In SPIE Smart Structures and Materials+ Nondestructive Evaluation and Health Monitoring* (pp. 94353I-94353I). International Society for Optics and Photonics.

[30] Kong, X., Li, J., Bennett, C., Collins, W., & Laflamme, S. (2016). Numerical simulation and experimental validation of a large-area capacitive strain sensor for fatigue crack monitoring. *Measurement Science and Technology*, **27**(12), 124009.

[31] Ubertini, F., Laflamme, S., Ceylan, H., Materazzi, A. L., Cerni, G., Saleem, H., ... & Corradini, A. (2014). Novel nanocomposite technologies for dynamic monitoring of structures: a comparison between cement-based embeddable and soft elastomeric surface sensors. *Smart Materials and Structures*, **23**(4), 045023.

[32] Cai, L., Song, L., Luan, P., Zhang, Q., Zhang, N., Gao, Q., ... & Zhou, W. (2013). Super-stretchable, transparent carbon nanotube-based capacitive strain sensors for human motion detection. *Scientific reports*, 3, 3048.

[33] Kang, I., Schulz, M. J., Kim, J. H., Shanov, V., & Shi, D. (2006). A carbon nanotube strain sensor for structural health monitoring. *Smart materials and structures*, **15**(3), 737.

[34] Gupta, S., & Ray, A. (2007). Real-time fatigue life estimation in mechanical structures. *Measurement Science and Technology*, **18**(7), 1947.

[35] ASTM International. (2015). Standard test method for measurement of fracture toughness. ASTM International.

[36] Kong, X., Li, J., Collins, W., Bennett, C., Laflamme, S., & Jo, H. (2017, April). A robust signal processing method for quantitative high-cycle fatigue crack monitoring using soft elastomeric capacitor sensors. *In SPIE Smart Structures and Materials+ Nondestructive Evaluation and Health Monitoring* (pp. 101680B-101680B). International Society for Optics and Photonics.